14TH CANADIAN MASONRY SYMPOSIUM
MONTREAL, CANADA
MAY 16TH – MAY 20TH, 2021

NUMERICAL MODELLING OF A FLEXURAL ENERGY DISSIPATION DEVICE FOR CONTROLLED ROCKING MASONRY WALLS

East, Matthew[1]; Ezzeldin, Mohamed[2] and Wiebe, Lydell[3]

ABSTRACT

Steel flexural yielding arms can be an effective energy dissipation device for controlled rocking masonry walls. In controlled rocking masonry walls, uplift of the wall from the foundation is allowed in a way that can localize damage to externally mounted energy dissipation devices and subsequently minimize post-earthquake residual drifts. Recent testing at McMaster University investigated the ability of steel flexural yielding arms to serve as easily replaceable energy dissipation devices with the ability to simultaneously resist sliding demands. Based on this previous testing, the current study investigates how to capture the behaviour of such devices through a finite element model using OpenSees, with the purpose of integrating the component models of flexural yielding arms with models of controlled rocking masonry walls. The flexural arm modelling approach is validated against the experimental data in terms of material data from coupon tests and low cycle fatigue parameters based on the observed hysteretic response from the experiments. The developed model is then used to investigate the performance of a wide array of devices, beyond the initial series of tests. The results showed that the proposed design equations are accurate within the examined geometric configurations.

KEYWORDS: *seismic design, controlled rocking, reinforced masonry, energy dissipation device, numerical modelling*

[1] PhD Candidate, Department of Civil Engineering, McMaster University, Hamilton, ON, L8S 4L7, Canada, eastma@mcmaster.ca
[2] Assistant Professor, Department of Civil Engineering, McMaster University, Hamilton, ON, L8S 4L7, Canada, ezzeldms@mcmaster.ca
[3] Associate Professor, Department of Civil Engineering, McMaster University, Hamilton, ON, L8S 4L7, Canada, wiebel@mcmaster.ca

INTRODUCTION

Over the last few decades, a wide variety of research studies have been conducted to evaluate and enhance the performance of conventional masonry shear walls [1-7]. Despite this, these walls are still limited in their seismic applications due to the high level of damage they experience [8]. This damage is the result of flexural cracks developing in the tensile regions at the base of the wall. To address this, numerous studies have demonstrated that controlled rocking masonry walls (CRMWs) with post-tensioning strands can be an effective and economic alternative to conventional reinforced masonry shear walls [9-11]. While promising, these studies have been limited in further application due to the difficulty in detailing of the post-tensioning strands, as well as the low inherent damping of the system [10-12].

To address this, experimental work has been conducted by Li [13] to develop an energy dissipation device to be attached at the base of the wall in order to simplify the detailing of the system and provide supplemental damping. The device is steel flexural arm which dissipates energy through flexural yielding when the wall uplifts from the foundation. The idealized hysteretic response of this system is shown in Figure 1. These devices are intended to be used with a gravity-controlled system as shown in Figure 1, or as supplemental damping for a post tensioned CRMW.

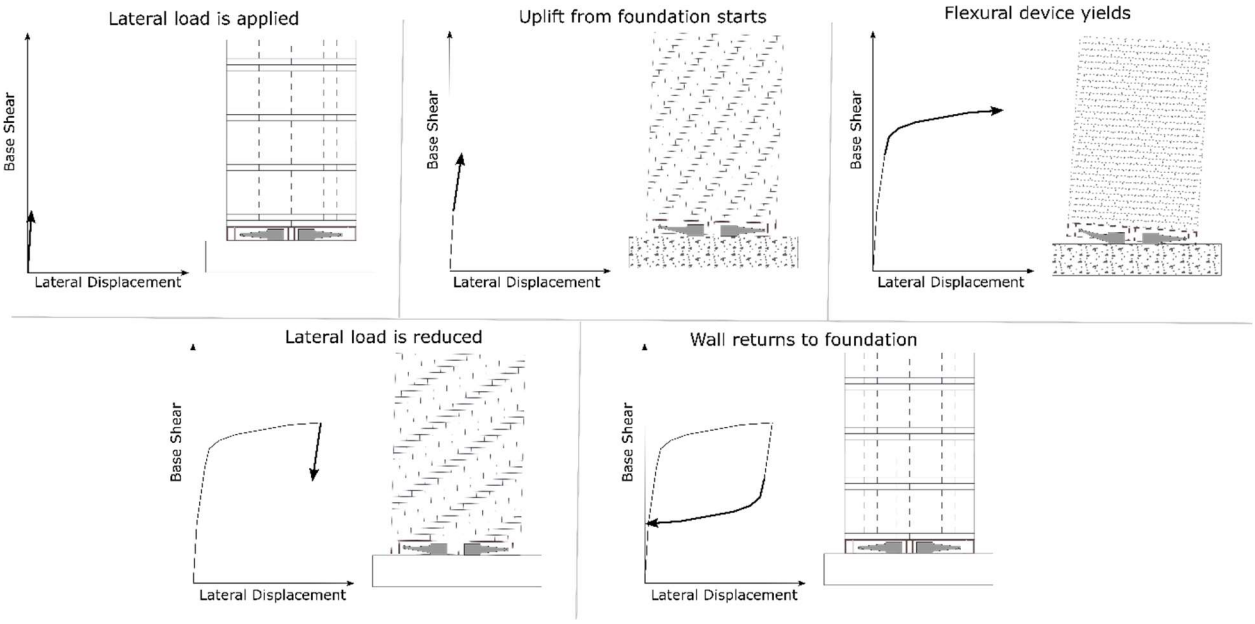

Figure 1: Hysteretic response of a CRMW system

Because the results of the tested devices are promising [13], a numerical model needs to be developed to further investigate the behaviour of these devices in a CRMW system and to develop further design guidelines for implementing them. The current study develops a 3D numerical model in OpenSees [14] using displacement-based elements and fiber sections to capture the behaviour of flexural yielding energy dissipation devices to be used in further numerical modelling of CRMWs with such devices.

SUMMARY OF THE EXPERIMENTAL WORK

Test Matrix

The numerical work developed in the current study is validated against the test results of thirteen steel flexural arms tested under displacement controlled quasi-static fully reversed cyclic loading by Li [13]. The experimental work consisted of two phases. Phase 1 investigated the flexural response of the devices with various lengths and aspect ratios (defined as the dimension b divided by the thickness t), while Phase 2 investigated the same geometric flexural arms, with the addition of an axial load of 30 kN. The test matrix is summarized in Table 1, as well as the corresponding material properties obtained from coupon tests.

Table 1: Test Matrix with Geometric Parameters and Mean Coupon Test Data

	ID	L (mm)	b/t	t (mm)	F_y (MPa)	F_u (MPa)
Aspect Ratio Phase 1	S-L1-4.3	315	4.3	22.23	400	563
	S-L1-5.0	315	5	19.05	400	562
	S-L1-6.0	315	6	15.88	400	555
	S-L1-7.5	315	7.5	12.7	508	545
Aspect Ratio Phase 2	S-L1-4.3A	315	4.3	22.23	399	563
	S-L1-5.0A	315	5	19.05	392	552
	S-L1-6.0A	315	6	15.88	390	539
	S-L1-7.5A	315	7.5	12.7	380	480
Length Phase 1	L-L1.4-6.0	440	6	15.88	392	542
	L-L1.2-6.0	380	6	15.88	392	551
	SL-L1-6.0	315	6	15.88	400	555
	L-L0.8-6.0	255	6	15.88	385	480
Length Phase 2	L-L1.4-6.0A	440	6	15.88	392	549
	L-L1.2-6.0A	380	6	15.88	395	555
	SL-L1-6.0A	315	6	15.88	390	539

The key dimensions of the devices are presented in Figure 2. The length was varied from 255 mm to 440 mm, while the aspect ratio (b/t) was varied from 4.3 to 7.5 by changing the thickness of the devices.

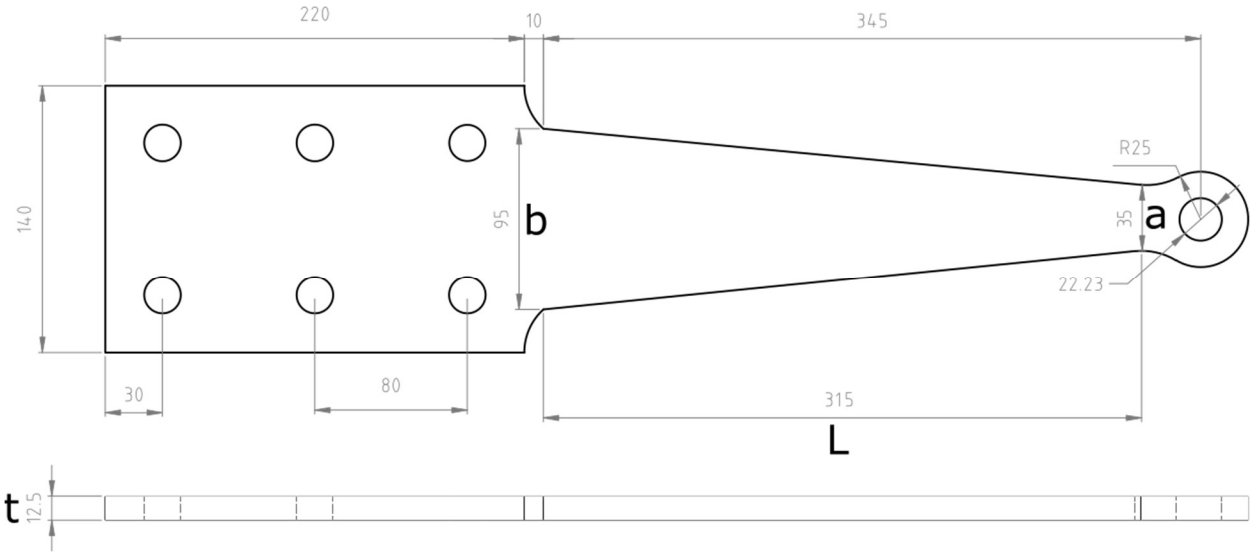

Figure 2: Flexural arm parameters (units in mm)

Test Setup

The test setup used is shown in Figure 3. The cyclic displacement was applied using a hydraulic actuator with a capacity of 120 kN and a maximum stroke of 90 mm in each direction, located to the north of the pinhole. Axial compression forces were applied using a hydraulic actuator with a capacity of 120 kN, located to the east of the pinhole.

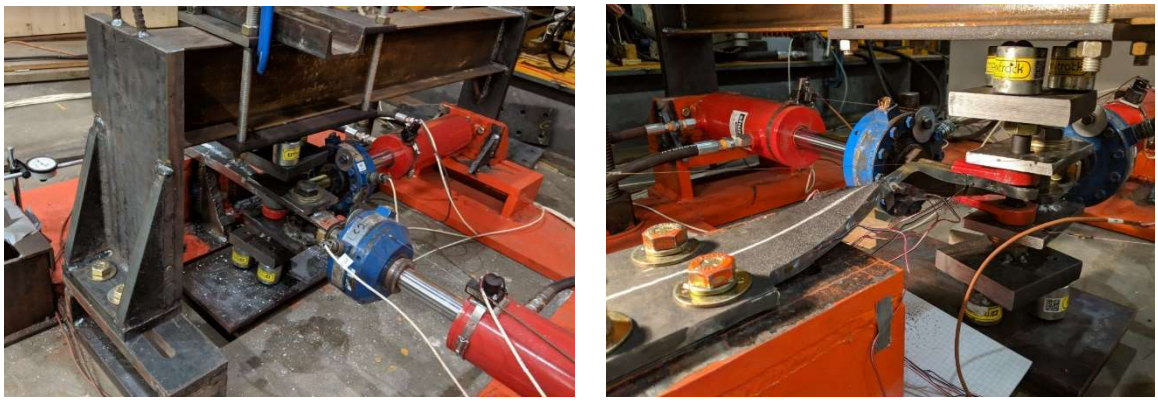

Figure 3: a.) Photo of Test Setup b.) Photo of Test Setup During Testing (Li 2019)

Loading Protocol

The displacement loading protocol was defined based on the FEMA 461 [15]. The target displacement was set to be 47 mm which corresponds to 3% drift of a reference wall. The displacement protocol followed FEMA 461 guidelines until the maximum stroke of the north displacement-controlled actuator (90mm) was reached [15]. Specimens were then subjected to maximum displacement cycles until 80% strength degradation or fracture was observed.

NUMERICAL MODELLING

A 3D nonlinear model of each specimen was created using the OpenSees software (Mazzoni et al. 2006). The model is constructed from 8 displacement-based beam column elements with fibre sections of decreasing size. The depth of each fiber section matches the average depth of the flexural arm over the length of that element. The thickness of the fiber sections matches the thickness of the flexural arm. The length corresponds to the length that may yield in flexure, shown as L in Figure 2.

The material properties were modelled using Steel02 available in OpenSees and calibrated from coupon tests conducted from the steel used for the devices. Low cycle fatigue was included through the Fatigue input within OpenSees with the Coffin-Mansen slope calibrated based on the experimental data (ranging between -0.352 and -0.454). The maximum strain obtained from the coupon tests was included to account for fracture of the devices. Figure 4 shows a schematic of the developed numerical model. P-Delta coordinate transformations were applied to ensure the axial load was applied properly throughout the analysis.

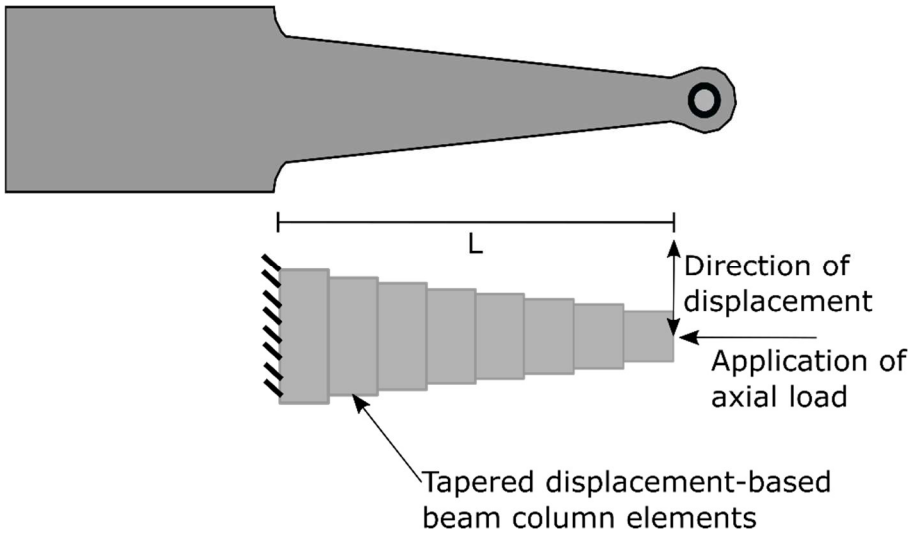

Figure 4: Model schematic (bottom) compared to flexural energy dissipation device (top)

COMPARISON BETWEEN NUMERICAL AND EXPERIMENTAL RESULTS

Figure 5 and 6 show the hysteretic response of the experimental results compared to that obtained from the OpenSees model. There is good agreement between the experimental hysteretic response observed and the equivalent result from the numerical model. The model adequately captures the influence of the axial load, as well as failure initiation due to low cycle fatigue fracture.

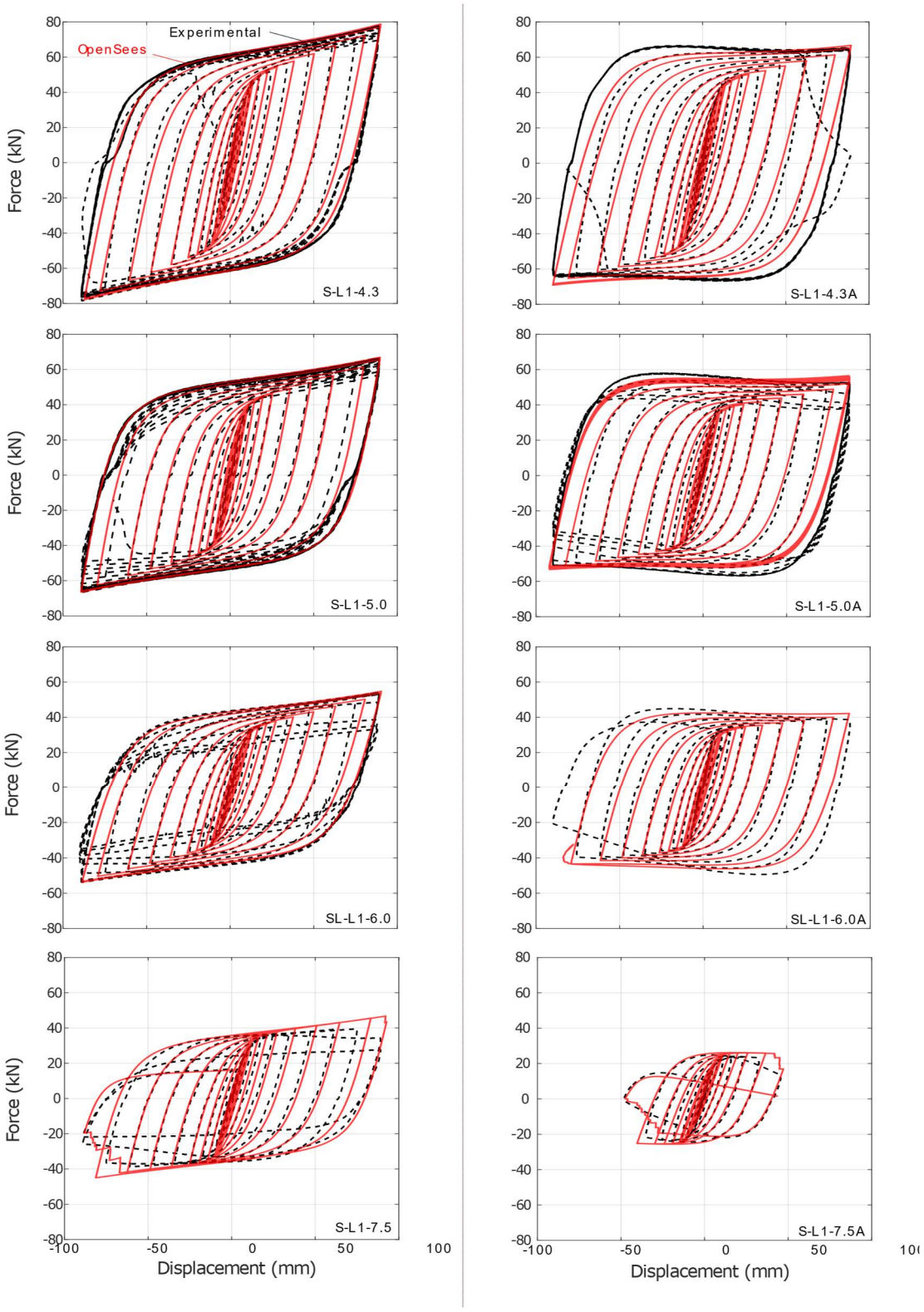

Figure 5: Experiemental and numerical hysteresis loops of flexural arms with varied aspect ratio

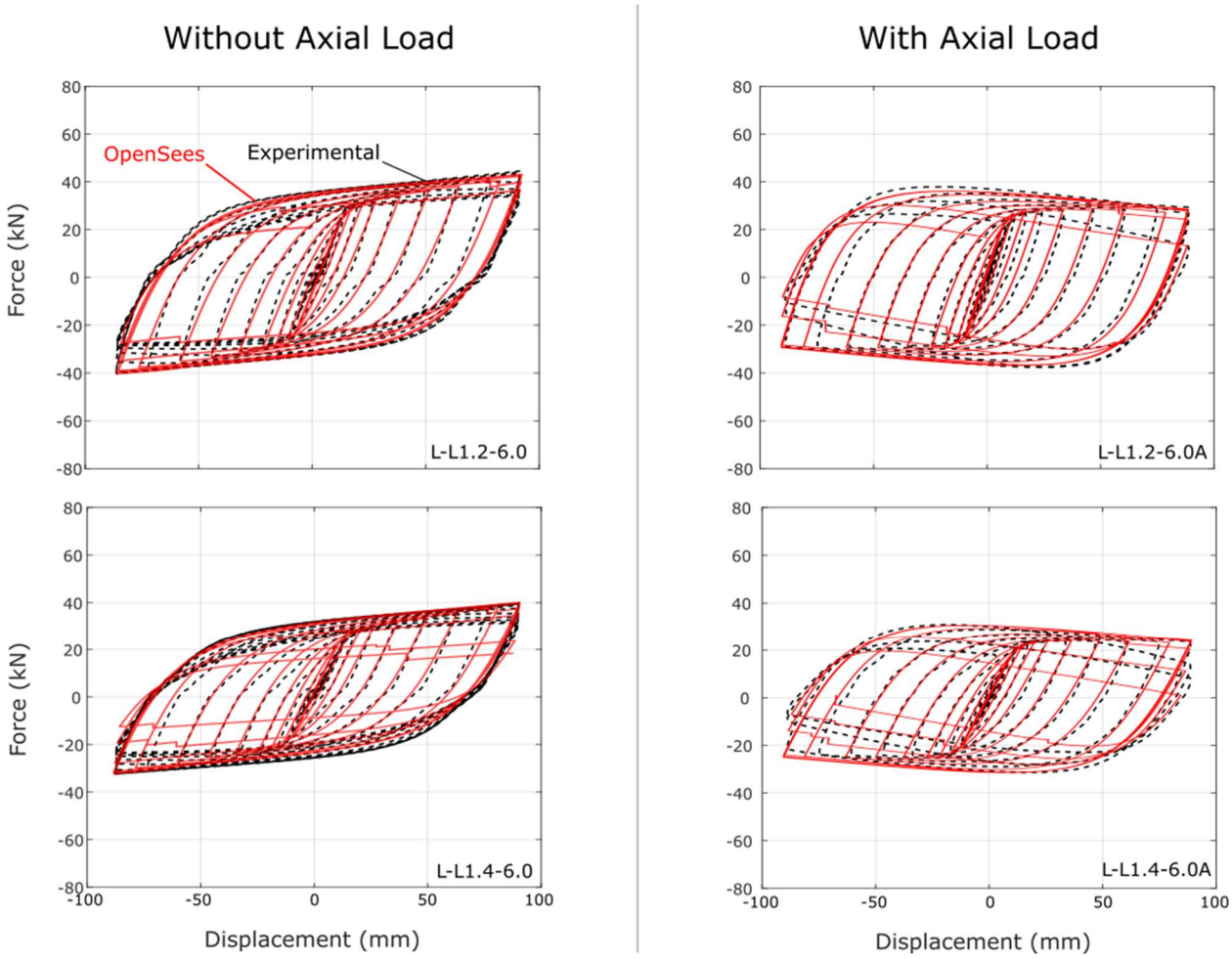

Figure 6: Experimental and numerical hysteresis loops of flexural arms with varied length

Energy Dissipation

The values for the cumulative energy dissipated were normalized by the total volume of the yielding steel for each specimen to obtain the effective energy dissipation performance per unit volume, thus facilitating the comparison between specimens with different geometric properties. Figure 7 shows the experimental and numerical cumulative energy dissipated as well as the cumulative displacement until failure of the experimental devices. The numerical model was used

to simulate flexural arms at lengths at 10 mm increments, as well as thicknesses at 6.25 mm increments.

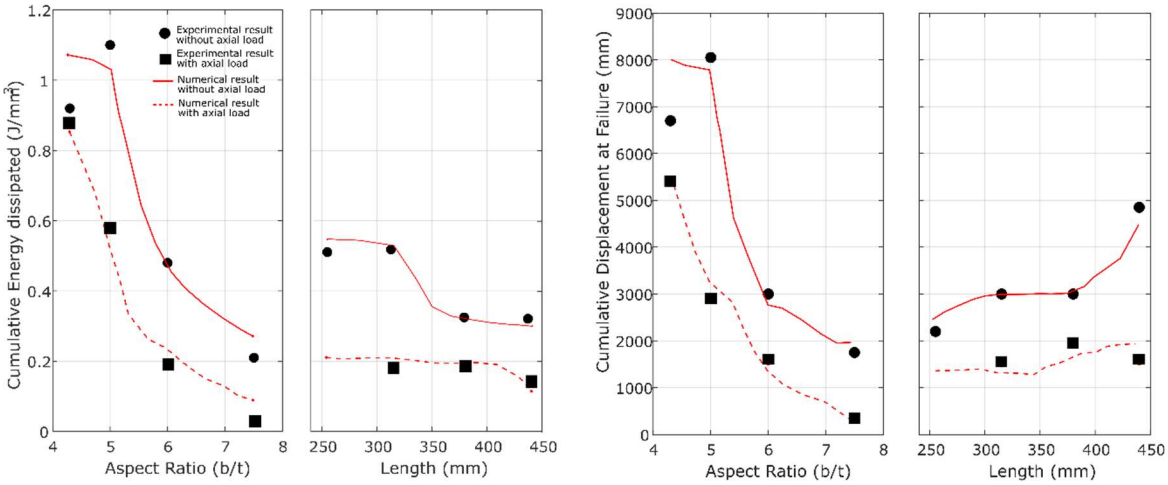

Figure 7: Cumulative energy dissipated and cumulative displacement

Table 2 summarizes the comparison of the numerical model (denoted as E_{dnum} and CD_{num}) to the experimental tests (denoted as E_{dexp} and CD_{exp}). The numerical model captured the energy dissipated to within 23% of the experimental results, while the cumulative displacement until failure was within 12% accurate.

Table 2: Comparison of experimental and numerical values for energy dissipation and cumulative displacement

ID	ED_{num}/ED_{exp}	CD_{num}/CD_{exp}
S-L1-7.5	1.14	1.06
S-L1-6.0	1.02	0.97
S-L1-5.0	0.97	0.96
S-L1-4.3	1.23	1.22
S-L1-7.5A	1.16	1.01
S-L1-6.0A	1.02	0.94
S-L1-5.0A	0.98	1.12
S-L1-4.3A	0.99	0.99
L-L0.8-6.0	1.04	1.05
SL-L1-6.0	1.02	0.97
L-L1.2-6.0	0.99	1.02
L-L1.4-6.0	0.98	0.95
SL-L1-6.0A	1.04	0.96
L-L1.2-6.0A	1.01	0.95
L-L1.4-6.0A	0.98	1.09

CONCLUSIONS

The current paper described the development of a 3D model using OpenSees to capture the behaviour of a flexural yielding device under combined cyclic loading and constant axial loading. These devices are intended to be used within controlled rocking masonry walls in future studies. Data from a previous experimental study was used to validate the developed numerical model, and it was found that the model was accurate in capturing the hysteretic response of the devices, as well as the displacement capacity and energy dissipated.

Ongoing research incorporates these devices into a controlled rocking masonry system to better understand the inelastic dynamic behaviour of controlled rocking masonry walls with supplemental energy dissipation devices.

ACKNOWLEDGEMENTS

The financial support for this project was provided through the Canadian Concrete Masonry Producers Association (CCMPA), the Canada Masonry Design Centre (CMDC), the Natural Sciences and Engineering Research Council (NSERC) and the Ontario Centres of Excellence (OCE).

REFERENCES

[1] Sveinsson, B. I., Sucuoglu, H., and McNiven, H. D. (1985). "Cyclic loading tests of masonry single piers - Volume 4: Additional tests with height to width ratio of 1." Report No. UCB/EERC-85/15, Earthquake Engineering Research Centre, University of California, Berkeley, CA.

[2] Matsumura, A. (1986). "Shear strength of reinforced hollow unit masonry walls." 2nd Meeting of the U.S.-Japan Joint Technical Coordinating Committee on Masonry Research, U.S. Japan Cooperative Research Program, CO.

[3] Kaminosono, T., Teshigowara, M., Hiraishi, H., Fujisawa, M., and Nakaoka, A. (1988). "Experimental study on seismic performance of reinforced masonry walls." Proc., *9th World Conf. on Earthquake Engineering, Japan Association for Earthquake Disaster Prevention*, Japan, pp. 109–114.

[4] Shing, P., Schuller, M., and Hoskere, V. (1990). "In-plane resistance of reinforced masonry shear walls." *Journal of Structural Engineering*, ASCE, Vol. 116, No.3, pp. 619–640.

[5] Voon, K., and Ingham, J. (2006). "Experimental in-plane shear strength investigation of reinforced concrete masonry walls." *Journal of Structural Engineering*, ASCE, Vol. 132, No.3, pp. 400–408.

[6] Seif ElDin, H. M., & Galal, K. (2017). In-plane seismic performance of fully grouted reinforced masonry shear walls. *Journal of Structural Engineering*, *143*(7), 04017054.

[7] Ezzeldin, M., El-Dakhakhni, W., & Wiebe, L. (2017). Experimental assessment of the system-level seismic performance of an asymmetrical reinforced concrete block–wall building with boundary elements. *Journal of Structural Engineering*, *143*(8), 04017063.

[8] EERI (2005). World housing project; Retrieved from http://www.world-housing.net/

[9] Toranzo, L. A. (2002). ''The use of rocking walls in confined masonry structures: a performance-based approach.'' *Ph.D. Dissertation*, Department of Civil Engineering, University of Canterbury, New Zealand.

[10] Toranzo, L. A., Restrepo, J. I., Carr, A. J., and Mander, J. B. (2004). “Rocking confined masonry walls with hysteretic energy dissipators and shake-table validation.” *Proc. 13th World Conference on Earthquake Engineering*, Paper No.248.
[11] Laursen, P. T. and Ingham, J. M. (2004). “Structural Testing of Enhanced Post-Tensioned Concrete Masonry Walls.” *Journal of Structural Engineering, ASCE*, Vol. 130, No.10, pp. 1497-1505.
[12] Hassanli, R., M. A. ElGawady, M.A., and Mills, J. E. (2017). "In-plane flexural strength of unbonded post-tensioned concrete masonry walls," *Engineering Structures,* 136, 245-260.
[13] J. Li. (2019) *Development of a flexural yielding energy dissipation device for controlled rocking masonry walls,* MASc Thesis: McMaster University.
[14] Mazzoni, S., McKenna, F., Scott, M. H., and Fenves, G. L. (2006). OpenSees Command Language Manual, Pacific Earthquake Engineering Research (PEER) Center.
[15] Federal Emergency Management Agency (FEMA). (2007). Interim Testing Protocols for Determining the Seismic Performance Characteristics of Structural and Nonstructural Components, Report No. FEMA-461.